Description of droplet coalescence and breakup in emulsions through a homogeneous population balance model

Simone Castellano, Nida Sheibat-Othman, Daniele L. Marchisio, Antonio Buffo, Sophie Charton

Description of droplet coalescence and breakup in emulsions through a homogeneous Population Balance Model

Simone Castellano[1,2], Nida Sheibat-Othman[2], Daniele Marchisio[3],

Antonio Buffo[3] and Sophie Charton[1]*

[1] CEA, DEN, Research Department of Mining and Fuel Recycling Processes, SA2I, FR-30207, Bagnols-sur-Cèze, France

[2] Université Claude Bernard Lyon 1,CNRS, UMR 5007, LAGEP, 43 bd 11 Novembre 1918, FR-69622 Villeurbanne, France

[3] Politecnico di Torino, Dipartimento di Scienza Applicate e Tecnologie, Corso Duca degli Abruzzi 24, IT-10129, Torino, Italy

* *Corresponding author:* sophie.charton@cea.fr

Abstract

A zero-dimensional homogenous Population Balance Model (PBM) based on the evaluation of the volume-averaged coalescence and breakup rates is here adopted for the first time to fit the model parameter values through experiments carried out on a water-oil emulsion. The method accounts for the spatial inhomogeneities in mixing, namely for the probability density function of the turbulent kinetic energy dissipation in the apparatus, but avoids the use of coupling the PBM with computational fluid dynamics (CFD) or compartmentalization, thus ensuring fast computational time. In order to demonstrate the advantage of the proposed model over traditional ones based on the volume-averaged turbulent kinetic energy dissipation rate, the operating conditions were varied, including the mixing rate, the disperse phase fraction as well as considering inverse emulsions (water in oil and oil in water). The new model was found to be more generalizable to different operating conditions.

Keywords:

Liquid-liquid emulsification, population balance modelling, turbulent dissipation rate, breakup and coalescence, probability density function, computational fluid dynamics

1 Introduction

Turbulent liquid-liquid dispersions are commonly present in chemical, nuclear, pharmaceutical and mining industries. Indeed, many unit operations involve the contact of two immiscible liquid phases, where one of the phases is dispersed in the form of droplets in the second one. In some applications, liquid-liquid emulsions, as well as gas-liquid dispersions, may involve mass transfer between the phases. In this case, turbulent flows are generally preferred as they provide a significant enhancement of the mass transfer rates. This is due to two distinct effects: the formation of smaller droplets, which give rise to a higher interfacial area between the two phases, and the continuous arrival of "fresh" eddies at the droplet surface, which increases the mass transfer coefficient.

In the industrial practice, the estimation of the droplet Sauter mean diameter at equilibrium is usually carried out by using empirical correlations, both in stirred tank reactors [1–3], and in extraction columns [4]. However, these correlations generally present the drawbacks of being valid only for similar geometrical and hydrodynamic conditions. Moreover, they are not appropriate to predict the transient behavior of this property.

Population balance equations (PBE) represent a step further in the prediction of the droplet size distribution (DSD) [5]. These equations were particularly useful for determining some relevant macroscopic properties as the interfacial area [6,7]. PBE requires the formulation of source terms to estimate breakage and coalescence frequencies. However, due to complex and multiscale phenomena involved, all the coalescence [8,9] and breakage [9–14] kernels proposed so far, involve empirical parameters that require numerical fitting on experimental data. It is important to highlight that most of these kernels are based on Kolmogorov's isotropic turbulence theory [15,16], which relates the flow characteristics to the turbulent kinetic energy dissipation rate, ε, in a liquid-liquid contactor.

(1.1) Since the Kolmogorov's theory is valid for high Reynolds number flows, the coalescence and breakage kernels may be applied in cases of fully developed turbulent flows.

Coulaloglou and Tavlarides [9] proposed kernels for droplet coalescence and breakage and identified a set of parameters for a liquid-liquid emulsion in a stirred tank. To this end, they considered a uniform value (*i.e.*, a volume-averaged value) of the turbulent dissipation rate when performing parameter identification from experimental data. Using this model, other studies followed, and various numerical values were provided for these parameters [17,18]. Amokrane et al. [6], and Becker et al. [19] showed that these estimated parameters could not be generalized from one device to another for systems with the same chemical components, indicating the possible necessity to better account for the hydrodynamics of the device in the kernel expression.

The assumption of uniform turbulence is indeed a rough approximation, as evidenced by experimental and simulation fluid flow investigations, which highlighted that the dissipation rate is several orders of magnitude higher near the impeller than in the recirculation zone [20–22]. Therefore, proper simulation of dispersed liquid-liquid flow would require two-way coupled CFD-PBE simulation. However, this method requires a very large computational time. In order to minimize the CPU costs, PBE solution methods based on calculating the moments of the DSD were developed [23,24]. The use of such two-way coupling may be useful for validation, but it remains limited to investigating particularly short process times, as the computation time may remain significant, hindering its use for simulating long time emulsification processes.

To address this issue, Alopaeus et al. [25] and Konno et al. [26] implemented a multiblock model to perform parameter identification. This method consisted in dividing the stirred tank reactor into subdomains where a uniform value of the turbulent kinetic energy dissipation rate is evaluated from a detailed CFD simulation. Although such compartmental models allowed a better representation of the turbulence in the reactor compared to a single volume-averaged value, the knowledge of additional terms representing the droplet fluxes among the subdomains is needed and retrieving this information from CFD simulations can be not trivial.

Alternatively, Buffo et al. [27] proposed an original and simplified method to account for the turbulence inhomogeneity for such systems. This method is based on the use of the probability

density function (pdf) of the turbulent dissipation rate, ε, in the liquid-liquid contactor to solve the PBE. The authors showed that this pdf of ε can be obtained from single- or multi-phase CFD simulations and a good agreement with fully detailed 3D CFD-PBE simulations can be obtained, especially when the mixing timescale is shorter than the characteristic coalescence and breakage timescales and the global volume fraction of the disperse phase is low. With this method the spatial dimensionality of the problem will remain 0D, while the dependence on ε is properly accounted for and should be appropriate for kernel parameter identification.

The aim of this work is to apply the method formulated by Buffo et al. [27] for predicting the behavior of a real liquid-liquid contactor, for which experimental measurements are performed. By using this methodology, new parameters of the coalescence and breakup models are identified for the investigated system, which would enable transferring of these to different operating conditions, equipment size and contactor technologies. Various new emulsification experiments were performed in a lab-scale stirred-tank reactor considering a system composed of distilled water and an organic phase, *i.e.* Isane 175, working under different stirring rates and using different disperse phase concentrations, to evaluate the behavior of the emulsion in time. More importantly, both the direct and the reverse emulsions were realized, to ensure that the model is accounting correctly for the physical-chemical emulsion properties without need for new parameter fitting. Full 3D CFD simulations of the experimental set were done to assess the pdf of ε achieved for each power input. The kernel parameters were identified using this method, and were compared to the parameters determined considering a uniform turbulent kinetic energy dissipation rate, ε, thus highlighting the relevance of such volume-averaged kernels for the simulation of liquid-liquid contactors.

2 Population Balance Modelling

The PBE is, in general, an integro-differential equation describing the evolution in time of the number density function (NDF). For non-uniform domains, *i.e.* when strong spatial gradients of the NDF are present, PBE can be stated as follows [28]:

$$\frac{\partial n(\boldsymbol{x},\boldsymbol{\varphi},t)}{\partial t}+\langle u_i\rangle\frac{\partial n(\boldsymbol{x},\boldsymbol{\varphi},t)}{\partial x_i}-\frac{\partial}{\partial x_i}\left[D_t\frac{\partial n(\boldsymbol{x},\boldsymbol{\varphi},t)}{\partial x_i}\right]=\frac{\partial}{\partial \varphi_j}\left[n(\boldsymbol{x},\boldsymbol{\varphi},t)\dot{\varphi}_J\right]+s(\boldsymbol{x},\boldsymbol{\varphi},t). \quad (1)$$

The reader should note that $\boldsymbol{x}$ and t are usually referred to as external coordinates, while the properties of the disperse phase considered in the generic vector $\boldsymbol{\varphi}$ as internal coordinates of the PBE. In this work, since the property of interest is only the interfacial surface, a number density function whose only internal coordinate is the droplet volume ($\boldsymbol{\varphi}=v$) is considered. For this simpler case, the net introduction of droplets in the system due to breakage and coalescence can be expressed as:

$$\begin{aligned}s(\boldsymbol{x},v,t)=&\int_v^\infty p(v')\,\beta(v|v')\Gamma(\boldsymbol{x},v')n(v',t)dv'-\Gamma(\boldsymbol{x},v)n(v,t)\\&+\frac{1}{2}\int_0^v Q(\boldsymbol{x},v-v',v')\,n(v-v',t)n(v',t)dv'\\&-n(v,t)\int_0^\infty Q(\boldsymbol{x},v,v')n(v',t).\end{aligned} \quad (2)$$

As previously mentioned, the most accurate method for assessing the dispersion behavior consists in considering the spatial distribution of the NDF and evaluating the velocity of the dispersion $\langle u_i\rangle$, using a coupled 3D CFD-PBM model. In this method mass, momentum and population balances need to be solved in each cell of the discretized domain, determining the temporal and spatial distribution of the NDF and of the flow characteristics. The knowledge of these quantities is of fundamental importance since the coalescence and breakage rates strongly depend on the fluid dynamics of the system. However, such coupled methods are not appropriate when the aim of the simulation is the identification of kernel parameters, since an optimization procedure implemented in this method is highly time-consuming [29].

As previously mentioned, the method proposed by Buffo et al. [27] can be used for this purpose. The computation of volume-averaged kernels through the probability density function of the turbulent dissipation rate appears to be a convenient compromise between computation time and accuracy. For a detailed derivation of the method, the reader can refer to the original work [27]. Here

the main governing equations are reported. **(1.2)** A homogeneous number density function is assumed in the contactor, defined as:

$$\bar{n}(v,t) = \frac{1}{V}\int_V n(\boldsymbol{x},v,t)d\boldsymbol{x} \tag{3}$$

this assumption leads to the following population balance equation (growth term is considered null since no mass transfer takes place between immiscible phases):

$$\frac{\partial \bar{n}(v,t)}{\partial t} = \int_v^\infty \bar{\Gamma}(v')\,\beta(v|v')\bar{n}(v',t)dv' - \bar{\Gamma}(v)\bar{n}(v,t) + \frac{1}{2}\int_0^v \bar{Q}(v,v')\,\bar{n}(v-v',t)\bar{n}(v',t)dv'$$

$$- \ \bar{n}(v,t)\int_0^\infty \bar{Q}(v,v')\bar{n}(v',t) \tag{4}$$

where the volume-averaged breakage and coalescence kernels, $\bar{\Gamma}(v)$ and $\bar{Q}(v,v')$ respectively, can be evaluated in the following way:

$$\bar{\Gamma}(v) = \frac{1}{V}\int_V \Gamma(\boldsymbol{x},v)d\boldsymbol{x} = \int_0^\infty \Gamma(\varepsilon,v)f(\varepsilon)d\varepsilon, \tag{5}$$

$$\bar{Q}(v,v') = \frac{1}{V}\int_V Q(\boldsymbol{x},v,v')d\boldsymbol{x} = \int_0^\infty Q(\varepsilon,v,v')f(\varepsilon)d\varepsilon. \tag{6}$$

where $f(\varepsilon)$ is the turbulent kinetic energy dissipation rate distribution in the system, to be evaluating through a detailed CFD simulation.

The reader should note that this 0D model presents the advantage of accounting for the turbulent non-uniformities, and the influence that these have on the breakage and coalescence rates in a 0-dimensional frame, with significant reduction of the computational time, compared to fully coupled CFD-PBM simulations. However, it is worth remarking that this method is applicable only when the NDF is spatially uniform, namely in dilute systems at low volume fractions of the disperse phase and at high stirring rates [27].

Moreover, it is important to mention that the most widely adopted approach in the literature considers instead a volume-averaged turbulent kinetic energy dissipation rate, $\bar{\varepsilon}$, as done by Coulaloglou and Tavlarides [9] to determine the parameters of their model. The reader should note that this method, unlike the 0D method using the pdf of ε adopted in this work, does not account for turbulent inhomogeneities in the apparatus. This means that, for example, experiments performed in

different vessels, characterized by completely different flow and turbulent fields and giving rise to very different DSDs, but resulting in the same volume-averaged turbulent dissipation rates, would result in identical predicted DSD evolutions.

2.1 Breakage and Coalescence kernels

Many models for breakage and coalescence kernels have been proposed in literature [30,31]. The Coulaloglou and Tavlarides kernels [9] remain the most widely used due to their simplicity and fundamental basis. Amokrane et al. [6] showed that Coulaloglou and Tavlarides kernels allow quite good fits to experimental data on emulsions performed in stirred tank reactors and pulsed columns, though with a need to refit the parameters when changing the apparatus or the emulsion itself (which is usually the case for other kernels too). For this reason, Coulaloglou and Tavlarides models are considered in this work.

In developing the breakage model, Coulaloglou and Tavlarides assumed the flow to be turbulent, and turbulence to be locally isotropic. The authors expressed *Γ(d)*, the breakage frequency of a droplet of diameter *d*, as follows:

$$\Gamma(d) = \frac{1}{t_b}\frac{N_{break}(d)}{N_{tot}(d)} \tag{10}$$

The fraction of breaking droplets depends on the surface energy of the droplets and the kinetic energy of the eddies in the turbulent flow:

$$\frac{N_{break}(d)}{N_{tot}(d)} = e^{-\frac{E_{surface,drop(d)}}{E_{kinetic,eddy}(d)}} = exp\left(-\frac{C_2\sigma}{\rho_d \varepsilon^{\frac{2}{3}} d^{-\frac{7}{3}}}\right) \tag{11}$$

It is important to remark that this model does not consider the viscous forces that oppose droplet rupture, namely when the viscosity of the disperse phase is low, as in the case of water and Isane 175.

The authors considered that the droplet breakage time, can be obtained by considering the relative motion of two lumps of fluid in the turbulent flow. Assuming the dimension of droplets to be in the inertial subrange, the breakage time is:

$$t_b = c_0\, \varepsilon^{-\frac{1}{3}} d^{\frac{2}{3}} \tag{12}$$

Including the damping effect due to disperse phase fraction on the turbulent dissipation rate, $\varepsilon_{eff} = \frac{\varepsilon}{(1+\phi)^3}$, the breakage frequency reads:

$$\Gamma(d) = \frac{C_1 \varepsilon^{\frac{1}{3}}}{(1+\phi)} d^{-\frac{2}{3}} exp\left(-\frac{C_2 \sigma (1+\phi)^2}{\rho_d \varepsilon^{\frac{2}{3}} d^{-\frac{7}{3}}}\right) \tag{13}$$

This breakage kernel contains two parameters, C_1 and C_2 that have to be determined through fitting to experimental data. It is important to remark that when the disperse phase volume fraction is low the damping effect is negligible.

To complete the breakage rate calculations, a daughter size distribution function is needed. **(2.1)** In literature, many functions were proposed for estimating the daughter size probability from a breakage event [30]. In this work, the normal distribution proposed by Valentas [32], and employed by Coulaloglou and Tavlarides was considered. This function, giving a higher probability for the formation of two equi-sized daughter droplets, is consistent with previous experimental observations [29].

The coalescence kernel proposed by Coulaloglou and Tavlarides expresses the coalescence frequency as the product of a collision frequency, h, and a coalescence efficiency, λ. The collision frequency is modeled assuming the droplet collisions to be analogous to molecule collisions in an ideal gas [33]:

$$h(v, v') = C_3 \varepsilon^{1/3} \left(v^{\frac{2}{3}} + v'^{\frac{2}{3}}\right)\left(v^{\frac{2}{9}} + v'^{\frac{2}{9}}\right)^{1/2} \tag{14}$$

Derivation of the coalescence efficiency is based on the film drainage theory of Shinnar and Church [34]:

$$\lambda(v, v') = \exp\left(-\frac{C_4 \mu_c \rho_c \varepsilon}{\sigma^2}\left(\frac{v^{\frac{1}{3}} v'^{\frac{1}{3}}}{v^{\frac{1}{3}} + v'^{\frac{1}{3}}}\right)^4\right) \tag{15}$$

Final expression of the coalescence kernel is:

$$Q(v,v') = C_3\varepsilon^{1/3}\left(v^{\frac{2}{3}} + v'^{\frac{2}{3}}\right)\left(v^{\frac{2}{9}} + v'^{\frac{2}{9}}\right)^{1/2} \exp\left(-\frac{C_4\mu_c\rho_c\varepsilon}{\sigma^2}\left(\frac{v^{\frac{1}{3}}v'^{\frac{1}{3}}}{v^{\frac{1}{3}} + v'^{\frac{1}{3}}}\right)^4\right) \quad (16)$$

As for the breakage kernel, two parameters, C_3 and C_4 have to be determined.

2.2 Numerical solution of PBE

As analytical solution for population balance equation is possible only for few simple cases [35,36], there are various numerical methods to solve PBE. Among these, class methods [37–39] and quadrature-based method of moments [23,24] have great importance.

Kumar and Ramkrishna [39] proposed the fixed pivot technique to solve the PBE involving breakage and coalescence. They integrated the PBE (Eq. 4) in each interval of the discretization, [v_i, v_{i+1}], to obtain a set of ordinary differential equations expressing the variation of the droplet number in each interval:

$$\begin{aligned}\frac{dN_i(t)}{dt} = & \sum_{\substack{j,k \\ p_{i-1}\le(p_j+p_k)\le p_{i+1}}}^{j\ge k}\left(1-\frac{1}{2}\delta_{j,k}\right)\eta\, Q_{j,k}N_j(t)N_k(t) - \Gamma_i N_i(t) \\ & -N_i(t)\sum_{k=1}^{M} Q_{i,k}N_k(t) + \sum_{k=1}^{M} m_{i,k}\,\Gamma_k N_k(t)\end{aligned} \quad (17)$$

where:

$$\eta = \begin{cases}\dfrac{p_{i+1}-v}{p_{i+1}-p_i} & p_i \le v \le p_{i+1} \\ \dfrac{v-p_{i-1}}{p_i-p_{i-1}} & p_{i-1} \le v \le p_i\end{cases} \quad (18)$$

and:

$$m_{i,k} = \int_{x_i}^{x_{i+1}} \frac{p_{i+1}-v}{p_{i+1}-p_i}\beta(v,p_k)dv + \int_{p_{i-1}}^{p_i} \frac{v-p_{i-1}}{p_i-p_{i-1}}\beta(v,p_k)dv \quad (19)$$

The Fixed Pivot method was implemented in a Matlab routine. The set of ordinary differential equations were solved using the ode15s function. The parameter identification was carried out using the pattern-search function (Global optimization toolbox of Matlab). **(1.1)** The optimization took approximately 15 minutes on an Intel Xeon dual-core machine (3.20 GHz) with 64GB of RAM.

Instead, to reproduce the evolution in time of the Sauter mean diameters for an emulsification experiment, once the parameters had been identified and the probability density function of ε had been implemented, the Matlab simulation took approximately 1 minute.

3 Materials and methods

3.1 Materials

Distilled water and Isane 175, provided by TOTAL, were used to prepare the emulsions. Isane 175 is a mixture of aliphatic and aromatic compounds with a number of carbon atoms between C12-C14. The physical properties of the liquids are given in Table 1.

No surfactant was used to stabilize the emulsion, therefore the surface tension is quite high, and coalescence may not be neglected even at low volume fractions. Both oil-in-water, at 1-2% volume fraction of Isane hold-up, and water-in-oil, at 1% volume fraction of water hold-up, dispersions were considered.

The emulsification experiments were performed in a 1-L stirred tank reactor. The tank diameter, T, is 120 mm, and its height, H, 120 mm. It is equipped with 4 baffles disposed symmetrically with respect to the reactor axis, with a width of 15 mm ($0.08T$) and a thickness of 5 mm. A 3-blade Mixel TT impeller has been employed (impeller diameter, D = 60 mm), located at 40 mm from the bottom of the reactor ($H/3$) characterized by a power number of Np = 0.81 for high Reynolds numbers [40].

The power number is a dimensionless coefficient which is dependent on the power introduced in the reactor, the fluid properties, the operating conditions and the geometrical constraints as follows:

$$N_p = \frac{P_w}{\rho N_r^3 D^5} \tag{20}$$

In case of a baffled reactor in which a turbulent flow is involved, the power number depends only on the geometry of the reactor, and not on the Reynolds number.

3.2 Experimental procedure

The experiments were carried out at different impeller rotational speeds (600-700-800 rpm) and hold-ups (1-2%). Both oil-in-water and water-in-oil dispersions were considered.

The experimental protocol consisted in filling the reactor with the required amounts of Isane and water (according to the required hold-up), and starting to stir at the required agitation speed. To monitor the droplet size distribution in the reactor, an endoscopic photo-optical device was employed (SOPAT® system). For each experiment, after 10 minutes from the start of the stirring, a first set of images was acquired to determine the initial drop size distribution. Then, the acquisition was repeated at different instants to obtain the DSD time evolution. The determination of the droplet size distributions from the acquired images was performed through image-processing software provided by SOPAT® (Fig. 1). For each acquisition, which lasted 60 s, with 4 images captured per second, the consistency of the number of the detected particles was checked, with regard to statistical relevance of the DSD [41]. From the DSD, the droplet Sauter mean diameter was computed as follows:

$$d_{32} = \frac{\int_0^\infty d^3 n(d) d(d)}{\int_0^\infty d^2 n(d) d(d)} \tag{21}$$

The Sauter mean diameter is expressed as the ratio between a term proportional to the total droplet volume (third moment of the distribution), which is constant, and a term proportional to the interfacial area (second moment of the droplet size distribution), which changes continuously as a result of droplet breakage and coalescence. Therefore, the higher the Sauter mean diameter, the lower will be the interfacial area between the two phases. This parameter is thus of great importance because it allows computation of the interfacial area, which is particularly useful when mass transfer occurs between the phases.

3.3 CFD model

The probability density function of the turbulent kinetic energy dissipation rate, ε, was obtained through CFD simulations using Ansys FLUENT®. Single phase simulations were run, assuming the effect of the dispersed diluted phase (1-2%) on the flow to be negligible.

The full 3D stirred tank reactor was meshed using Ansys Meshing. The mesh is unstructured and constituted of approximatively 2,000,000 tetrahedral cells, with an average orthogonal quality of 0.89 and a minimum of 0.25.

(3.1) In the simulations, the Multiple Reference Frame (MRF) technique was used to model the stirrer motion. The 3D stirred tank reactor was then divided into two cell zones: the first zone enclosing the fluid domain near the impeller, which directly experiences the stirrer motion (whose rotational speed is imposed as cell-zone condition); the second zone enclosing the remaining part of the fluid domain. At the interface between the two cell zones, the momentum fluxes are computed through appropriate mathematical transformation [42]. The MRF technique represents a good compromise between accuracy and computational costs, compared with other detailed methods such as the Sliding Mesh method [43].

As far as the turbulence modeling is concerned, the RANS approach was used. In particular, the standard k-epsilon model with enhanced wall treatment function was employed.

From preliminary steady–state CFD simulations, the convergence criteria, based on the absolute residual for each solved equation (set at 10^{-6}), were not reached. Therefore, transient simulations were run to obtain the probability density function of the turbulent dissipation rate. These simulations were run until the volume-averaged value of the turbulent dissipation rate was constant. **(1.2)** This operation took approximately 5 hours on an Intel Xeon dual-core machine (3.20 GHz) with 64GB of RAM: this time is considerably lower than the one required to perform a CFD-PBE simulation of the stirred tank reactor. Indeed, a CFD-PBE simulation requires the solution of additional equations, whose number depends on the method adopted for the PBE solution. Therefore, the CFD-PBE simulation may take several days to fully reproduce an emulsification experiment.

The time was discretized through a second order implicit method. The time step was set between 0.0002 s and 0.00025 s, according to the rotation speed of the moving cell zone. This time step allowed the convergence criteria to be reached in 15-20 iterations. Pressure, momentum, turbulent kinetic energy and turbulence dissipation rate were discretized through a second order upwind method. Pressure-velocity coupling was treated through the SIMPLE scheme.

4 Results and discussions

4.1 CFD simulation results

The probability density functions of the turbulent dissipation rate were determined through single-phase CFD simulations, employing either water or Isane alone at different rotation speeds. As expressed in Sec. 3.3, the transient simulations were run until a constant value of the volume-averaged turbulent dissipation rate was reached.

The probability density functions obtained for each operating condition at different rotational speeds were compared (Fig. 2). As expected, for both phases, higher impeller rotational speeds lead to higher probability that a large number of fluid elements experiences higher values of the turbulent dissipation rate. Indeed, it can be seen for instance that while stirring at 600 rpm, the probability of high turbulent energy dissipations is relatively low.

Also, the probability density functions obtained for water and the ones obtained for Isane are similar (Fig. 3). This is due to the fact that these products have quite similar viscosities, but differ in density, thus leading to similar dissipation of turbulent kinetic energy. Slight differences are present in the two functions at 600 rpm and 700 rpm, but at 800 rpm are almost identical. Both the functions obtained with water and those obtained with Isane will be used in parameter identification and model validation at the different conditions.

The volume average value of the turbulent dissipation rate in a stirred tank reactor can be computed as function of the power number (N_p) and geometrical and operating conditions:

$$\bar{\varepsilon} = \frac{P}{m_r} = \frac{N_p N^3 D^5}{V_r} \tag{26}$$

According to Eq. (26), the volume-averaged value of the turbulent dissipation rate depends on the volume of fluid present in the reactor, but not on the properties of the liquid (i.e. viscosity and density), **(4.1)** provided that the power number (N_p) of the impeller is constant.

The final volume-averaged values of the turbulent dissipation rates reached in the CFD simulations were found to be very similar to the ones computed using Eq. (26) (see Tab. 2). **(4.2)** However, slightly different turbulent dissipation rates were predicted employing water or Isane. The small differences may be explained considering changes in the power number, which is proportional to the turbulent dissipation rate. Indeed, the power number of an impeller is constant for high Reynolds numbers (more than 10^5), but it varies at lower Reynolds numbers [44]. Since both Isane

and water continuous-phase experiments are characterized by Reynolds numbers lower than 10^5 (Tab. 3), the predicted turbulent dissipation rates may differ. This supposition is also confirmed by the fact that, as the rotational speed of the impeller increases (and consequently the Reynolds number), the volume-averaged turbulent dissipation rates tend to the same values (Tab.2). Nevertheless, it is important to point out that the spatial distribution of the turbulent dissipation rate is far from being uniform in the reactor (Fig. 4). This property has high values in the proximity of the impeller, while it is lower in the recirculation zone. According to the division of the reactor in two different cell zones as reported in Sec. 3.3, the volume-averaged turbulent dissipation rate experienced by the fluid in the cell zone enclosing the impeller is 4-5 times the one experienced by the fluid in the rest of the reactor (Tab. 4).

4.2 Oil in water emulsions

As reported in Sec. 3.2, several emulsification experiments were performed changing the impeller rotational speed (600 to 800 rpm), the hold-up (1-2%) and inverting the continuous and disperse phases (Isane and water).

The experiments performed with water as continuous phase and 1-2% Isane hold-up showed that higher impeller rotational speeds lead to the generation of smaller droplets (Fig. 5). This is due to the higher input energy fed to turbulent eddies which causes higher velocity and pressure fluctuations that lead to the droplet breakage. However, while the difference between the droplet sizes obtained with 600 and 700 rpm stirring rate is quite high, the difference between 700 and 800 rpm stirring rate is much lower, indicating a hydrodynamic equilibrium between breakup and coalescence.

It is also interesting to point out that the higher the hold-up of the disperse phase, the bigger the Sauter mean diameter at the same impeller rotational speed. Indeed, higher Isane volume fraction increases the number of droplets present in the reactor, and therefore enhances the probability that two droplets collide and coalesce.

4.3 Water in Isane emulsion

The second set of experiments was performed employing Isane as continuous phase and 1% water hold-up. As in the previous case, smaller droplets were formed when the agitation in the reactor was higher (Fig. 6).

A comparison between the direct oil-in-water emulsion with the inverse emulsion is shown in Fig. 7. It can be seen that under the same stirring rate, water droplets were smaller than Isane droplets for stirring rates of 600 and 700 rpm. However, at 800 rpm stirring rate, both the direct and inverse emulsion led to similar droplet sizes of the disperse phase.

4.4 Identification of parameter values

The identification of the Coulaloglou and Tavlarides model parameters [9] was performed through the oil in water experiments at 600 rpm and 1-2 % volume fraction of Isane hold-up. The parameters were determined implementing the probability density functions of the turbulent dissipation rate obtained at 600 rpm and water as continuous phase. **(2.1)** The volume-averaged kernels were computed approximating the integrals of Eq. (5) and Eq. (6) by a classical numerical integration method:

$$\bar{\Gamma}(v) = \int_0^\infty \Gamma(\varepsilon, v) f(\varepsilon) d\varepsilon \approx \sum_{i=1}^{\infty} \Gamma(\varepsilon_i, v) f(\varepsilon_i) \left(\varepsilon_{\frac{i+1}{2}} - \varepsilon_{\frac{i}{2}} \right) \tag{27}$$

$$\bar{Q}(v, v') = \int_0^\infty Q(\varepsilon, v, v') f(\varepsilon) d\varepsilon \approx \sum_{i=1}^{\infty} Q(\varepsilon_i, v, v') f(\varepsilon_i) \left(\varepsilon_{\frac{i+1}{2}} - \varepsilon_{\frac{i}{2}} \right) \tag{28}$$

where $\Gamma(\varepsilon_i, v)$ and $Q(\varepsilon_i, v, v')$ are the breakage and coalescence kernels evaluated for $\varepsilon = \varepsilon_i$ and $f(\varepsilon_i)$ is the probability density value of ε_i extracted from the single-phase CFD simulation. Then, for the sake of comparison, these parameters were identified assuming a uniform value of the turbulent dissipation rate (0D PBE based on $\bar{\varepsilon}$ from Eq. 26).

The identification was carried out through a Matlab routine employing a global optimization procedure (*patternsearch* function). For each experiment, the function to be optimized was the sum

of the square differences between the simulated Sauter mean diameters, computed with a certain set of parameters, and the values obtained experimentally.

A good fitting of the experimental data was reached with both methods (see Fig. 8). However, the two sets of identified parameters differ (Tab. 5). It can be seen that when a uniform turbulent dissipation rate, $\bar{\varepsilon}$, is used, the identified breakage and coalescence parameters are respectively higher and lower than those obtained when employing the probability density function of ε. Indeed, this latter method accounts for the high values of the turbulent dissipation rate, which causes high breakage frequency, thus requiring lower values of the corresponding parameters.

4.5 Validation of parameter values

The two sets of identified parameters (using the pdf of ε, and volume-averaged $\bar{\varepsilon}$) in the selected experiments of Sec. 4.4 (at 600 rpm and using water as continuous phase, with different isane hold-ups) were tested with the experiments performed at higher impeller rotation speeds (700-800 rpm) as well as when inverting the phases (water-in-oil emulsion). The objective is to evaluate the accuracy of the model in cases of different turbulent conditions and breakage and coalescence rates (being these latter function of densities and viscosities of continuous and disperse phases), and to determine which set of parameters is more adequate, thus to decide which method between the one based on the pdf of ε and the one using $\bar{\varepsilon}$ is more generalizable to other apparatus or emulsification systems.

The first simulations dealt with the fitting of the experimental data at 700-800 rpm and 1-2 % volume fraction of Isane hold-up. For the four experiments (Fig. 9), the droplet Sauter diameters predicted employing the parameters identified with the homogeneous model with the probability density functions of the turbulent dissipation rate, are very similar to the experimental ones. This is not the case for the model results obtained using the parameters identified assuming the turbulent dissipation rate to be uniform (traditional method). The error obtained with this method seems to increase when the turbulence and the hold-up are higher. Indeed, the better hydrodynamic description given by the new model allows the transposition of the parameters for different turbulent conditions.

The second part of the parameter validation dealt with the experimental data obtained for the inverse emulsion, with water hold-up of 1%. As in the previous case, the parameters identified with

the new method along with the probability density functions of the turbulent dissipation rate gave better predictions than with the traditional method (Fig. 10). This demonstrates that the parameters obtained with the new model are generalizable to different hydrodynamic and chemical-physical conditions.

5 Conclusion

A 0D homogenous method that takes into account the non-uniformity of the turbulent kinetic energy dissipation rate, without employing a 3D description of the hydrodynamic (nor CFD-PBE coupling, or compartmentalization), was used for predicting the behavior of the Sauter mean diameter in a real liquid-liquid experiment. This method is based on the use of the probability density function of the dissipation rate ε into the population balance model, allowing the computation of a volume-averaged kernel, rather than using a volume-averaged value of this property as usually done in traditional 0D methods. With this methodology it was possible to evaluate the model parameters for the droplet coalescence and breakage models to be used to reproduce the experimental data under a wide range of operating condition.

The method (based on the pdf of ε) appeared to be more accurate than the traditional method (based on $\bar{\varepsilon}$). Indeed, the traditional 0D method represented a rough approximation of the real energy dissipation, due to the fact that this property is far from being uniform in the apparatus.

Parameters identification was performed using the experiments at 600 rpm and 1-2 % volume fraction of Isane in water, by employing both methods, through a global optimization algorithm. Later, the identified parameters for the two models were tested for new experimental data obtained at higher rotational speeds (700-800 rpm, 1-2 % volume fraction hold-up) as well as considering phase inversion (water-in-Isane, 1 % volume fraction hold-up). The model assuming a uniform turbulent dissipation rate failed to predict the Sauter mean diameters when the operating conditions were modified. The non-uniformity in the apparatus is indeed important and cannot be approximated through a uniform value of the turbulent dissipation energy. Instead, the model based on the computation of the volume-averaged kernel predicted the values of the Sauter diameter which fit accurately the experimental data, even when the hydrodynamic conditions were varied and when the

emulsion was inversed. This indicates that the obtained parameters would be more generalizable to different geometries of the system, stirring rates and disperse phase volume fraction.

Notation

C_1, C_2	breakage kernel parameters
C_3, C_4	coalescence kernel parameters
d	droplet diameter (m)
D	stirrer diameter (m)
D_t	diffusivity of disperse phase (m^2/s)
f	probability density function
$h(v,v')$	collision frequency
k	turbulent kinetic energy (m^2/s^2)
m_r	mass of fluid in the reactor (kg)
$n(v)$	number density function ($1/m^6$)
N	droplet number
N_p	Power number
N_r	rotational speed (tr/s)
p	pivot of i^{th} cell (m^3)
P	pressure (Pa)
P_w	dissipated power (W)
$Q(v,v')$	coalescence kernel (1/s)
$s(x,v,t)$	PBE source term ($1/(m^6 \cdot s)$)
t	time (s)
T	stirred tank diameter (m)
u	velocity of the continuous phase (m/s)

v	droplet volume (m^3)
V	volume of fluid (m^3)
$\boldsymbol{x}$	Cartesian space coordinates
β	daughter size distribution function
Γ	breakup kernel (1/s)
λ	collision efficiency
μ	viscosity (Pa·s)
μ_t	turbulent eddy viscosity (Pa·s)
ε	turbulent kinetic energy dissipation rate (m^2/s^3)
ρ	density (kg/m^3)
σ	interfacial tension (N/m)
$\boldsymbol{\varphi}$	disperse phase internal coordinates
$\boldsymbol{\phi}$	disperse phase fraction

Acknowledgments

This work was founded by the Nuclear Energy Division of CEA (program PAREC).

References

[1] R. Shinnar, On the behaviour of liquid dispersions in mixing vessels, J. Fluid Mech. 10 (1961) 259. doi:10.1017/S0022112061000214.

[2] F.B. Sprow, Distribution of drop sizes produced in turbulent liquid—liquid dispersion, Chem. Eng. Sci. 22 (1967) 435–442. doi:10.1016/0009-2509(67)80130-1.

[3] A.W. Pacek, C.C. Man, A.W. Nienow, On the Sauter mean diameter and size distributions in turbulent liquid/liquid dispersions in a stirred vessel, Chem. Eng. Sci. 53 (1998) 2005–2011. doi:10.1016/S0009-2509(98)00068-2.

[4] L. Boyadzhiev, M. Spassov, On the size of drops in pulsed and vibrating plate extraction columns, Chem. Eng. Sci. 37 (1982) 337–340. doi:10.1016/0009-2509(82)80169-3.

[5] D. Ramkrishna, Population balances: theory and applications to particulate systems in engineering, Academic Press, San Diego, CA, 2000.

[6] A. Amokrane, S. Charton, N. Sheibat-Othman, J. Becker, J.P. Klein, F. Puel, Development of a CFD-PBE coupled model for the simulation of the drops behaviour in a pulsed column, Can. J. Chem. Eng. 92 (2014) 220–233. doi:10.1002/cjce.21933.

[7] M.M. Attarakih, H.-J. Bart, N.M. Faqir, Numerical solution of the bivariate population balance equation for the interacting hydrodynamics and mass transfer in liquid–liquid extraction columns, Chem. Eng. Sci. 61 (2006) 113–123. doi:10.1016/j.ces.2004.12.055.

[8] H. Sovová, Breakage and coalescence of drops in a batch stirred vessel—II comparison of model and experiments, Chem. Eng. Sci. 36 (1981) 1567–1573. doi:10.1016/0009-2509(81)85117-2.

[9] C.A. Coulaloglou, L.L. Tavlarides, Description of interaction processes in agitated liquid-liquid dispersions, Chem. Eng. Sci. 32 (1977) 1289–1297. doi:10.1016/0009-2509(77)85023-9.

[10] T. Wang, J. Wang, Y. Jin, A novel theoretical breakup kernel function for bubbles/droplets in a turbulent flow, Chem. Eng. Sci. 58 (2003) 4629–4637. doi:10.1016/j.ces.2003.07.009.

[11] J. Baldyga, W. Podgórska, Drop break-up in intermittent turbulence: Maximum stable and transient sizes of drops, Can. J. Chem. Eng. 76 (1998) 456–470. doi:10.1002/cjce.5450760316.

[12] C. Martínez-Bazán, J.L. Montañés, J.C. Lasheras, On the breakup of an air bubble injected into a fully developed turbulent flow. Part 1. Breakup frequency, J. Fluid Mech. 401 (1999) 157–182. doi:10.1017/S0022112099006680.

[13] V. Alopaeus, J. Koskinen, K.I. Keskinen, Simulation of the population balances for liquid–liquid systems in a nonideal stirred tank. Part 1 Description and qualitative validation of the model, Chem. Eng. Sci. 54 (1999) 5887–5899. doi:10.1016/S0009-2509(99)00170-0.

[14] H. Luo, H.F. Svendsen, Theoretical model for drop and bubble breakup in turbulent dispersions, AIChE J. 42 (1996) 1225–1233. doi:10.1002/aic.690420505.

[15] A.N. Kolmogorov, A refinement of previous hypotheses concerning the local structure of turbulence in a viscous incompressible fluid at high Reynolds number, J. Fluid Mech. 13 (1962) 82. doi:10.1017/S0022112062000518.

[16] G.K. Batchelor, The theory of homogeneous turbulence, Cambridge Science Classic, Cambridge, 1953.

[17] J. Solsvik, P.J. Becker, N. Sheibat-Othman, H.A. Jakobsen, Population balance model: Breakage kernel parameter estimation to emulsification data, Can. J. Chem. Eng. 92 (2014) 1082–1099. doi:10.1002/cjce.21928.

[18] S. Maaß, M. Kraume, Determination of breakage rates using single drop experiments, Chem. Eng. Sci. 70 (2012) 146–164. doi:10.1016/j.ces.2011.08.027.

[19] P.J. Becker, F. Puel, R. Henry, N. Sheibat-Othman, Investigation of Discrete Population Balance Models and Breakage Kernels for Dilute Emulsification Systems, Ind. Eng. Chem. Res. 50 (2011) 11358–11374. doi:10.1021/ie2006033.

[20] M. Jenne, M. Reuss, A critical assessment on the use of k–ε turbulence models for simulation of the turbulent liquid flow induced by a Rushton-turbine in baffled stirred-tank reactors, Chem. Eng. Sci. 54 (1999) 3921–3941. doi:10.1016/S0009-2509(99)00093-7.

[21] J. Aubin, P. Mavros, D.F. Fletcher, J. Bertrand, C. Xuereb, Effect of Axial Agitator Configuration (Up-Pumping, Down-Pumping, Reverse Rotation) on Flow Patterns Generated in Stirred Vessels, Chem. Eng. Res. Des. 79 (2001) 845–856. doi:10.1205/02638760152721046.

[22] S. Baldi, M. Yianneskis, On the quantification of energy dissipation in the impeller stream of a stirred vessel from fluctuating velocity gradient measurements, Chem. Eng. Sci. 59 (2004) 2659–2671. doi:10.1016/j.ces.2004.03.021.

[23] D.L. Marchisio, R.D. Vigil, R.O. Fox, Quadrature method of moments for aggregation–breakage processes, J. Colloid Interface Sci. 258 (2003) 322–334. doi:10.1016/S0021-9797(02)00054-1.

[24] D.L. Marchisio, R.O. Fox, Solution of population balance equations using the direct quadrature method of moments, J. Aerosol Sci. 36 (2005) 43–73. doi:10.1016/j.jaerosci.2004.07.009.

[25] V. Alopaeus, J. Koskinen, K. I. Keskinen, J. Majander, Simulation of the population balances for liquid–liquid systems in a nonideal stirred tank. Part 2—parameter fitting and the use of the multiblock model for dense dispersions, Chem. Eng. Sci. 57 (2002) 1815–1825. doi:10.1016/S0009-2509(02)00067-2.

[26] M. Konno, M. Aoki, S. Saito, Scale effect on breakup process in liquid-liquid agitated tanks., J. Chem. Eng. Jpn. 16 (1983) 312–319. doi:10.1252/jcej.16.312.

[27] A. Buffo, J. De Bona, M. Vanni, D.L. Marchisio, Simplified volume-averaged models for liquid–liquid dispersions: Correct derivation and comparison with other approaches, Chem. Eng. Sci. 153 (2016) 382–393. doi:10.1016/j.ces.2016.07.032.

[28] D.L. Marchisio, J.T. Pikturna, R.O. Fox, R.D. Vigil, A.A. Barresi, Quadrature method of moments for population-balance equations, AIChE J. 49 (2003) 1266–1276. doi:10.1002/aic.690490517.

[29] A. Amokrane, S. Maaß, F. Lamadie, F. Puel, S. Charton, On droplets size distribution in a pulsed column. Part I: In-situ measurements and corresponding CFD–PBE simulations, Chem. Eng. J. 296 (2016) 366–376. doi:10.1016/j.cej.2016.03.089.

[30] Y. Liao, D. Lucas, A literature review on mechanisms and models for the coalescence process of fluid particles, Chem. Eng. Sci. 65 (2010) 2851–2864. doi:10.1016/j.ces.2010.02.020.

[31] J.C. Lasheras, C. Eastwood, C. Martínez-Bazán, J.L. Montañés, A review of statistical models for the break-up of an immiscible fluid immersed into a fully developed turbulent flow, Int. J. Multiph. Flow. 28 (2002) 247–278. doi:10.1016/S0301-9322(01)00046-5.

[32] K.J. Valentas, N.R. Amundson, Breakage and Coalescence in Dispersed Phase Systems, Ind. Eng. Chem. Fundam. 5 (1966) 533–542. doi:10.1021/i160020a018.

[33] E.H. Kennard, Kinetic Theory of Gases with an Introduction to Statistical Mechanics, McGraw-Hill, 1938.

[34] R. Shinnar, J.M. Church, Statistical Theories of Turbulence in Predicting Particle Size in Agitated Dispersions, Ind. Eng. Chem. 52 (1960) 253–256. doi:10.1021/ie50603a036.

[35] R.M. Ziff, New solutions to the fragmentation equation, J. Phys. Math. Gen. 24 (1991) 2821–2828. doi:10.1088/0305-4470/24/12/020.

[36] R.M. Ziff, E.D. McGrady, The kinetics of cluster fragmentation and depolymerisation, J. Phys. Math. Gen. 18 (1985) 3027–3037. doi:10.1088/0305-4470/18/15/026.

[37] F. Filbet, P. Laurençot, Numerical Simulation of the Smoluchowski Coagulation Equation, SIAM J. Sci. Comput. 25 (2004) 2004–2028. doi:10.1137/S1064827503429132.

[38] J. Kumar, M. Peglow, G. Warnecke, S. Heinrich, L. Mörl, Improved accuracy and convergence of discretized population balance for aggregation: The cell average technique, Chem. Eng. Sci. 61 (2006) 3327–3342. doi:10.1016/j.ces.2005.12.014.

[39] S. Kumar, D. Ramkrishna, On the solution of population balance equations by discretization—I. A fixed pivot technique, Chem. Eng. Sci. 51 (1996) 1311–1332. doi:10.1016/0009-2509(96)88489-2.

[40] I. Houcine, E. Plasari, R. David, Effects of the Stirred Tank's Design on Power Consumption and Mixing Time in Liquid Phase, Chem. Eng. Technol. 23 (2000) 605–613. doi:10.1002/1521-4125(200007)23:7<605::AID-CEAT605>3.0.CO;2-0.

[41] A. Buffo, V. Alopaeus, Experimental determination of size distributions: analyzing proper sample sizes, Meas. Sci. Technol. 27 (2016) 045301. doi:10.1088/0957-0233/27/4/045301.

[42] T. Ahmad, S.L. Plee, J.P. Myers, Fluent Theory Guide, ANSYS, Canonsburg, 2013.

[43] W. Bujalski, Z. Jaworski, A.W. Nienow, Cfd study of homogenization with dual rushton turbines—comparison with experimental results Part II: The Multiple Reference Frame, 80 (2002) 8.

[44] E.L. Paul, V.A. Atiemo-Obeng, S.M. Kresta, eds., Handbook of industrial mixing: science and practice, Wiley-Interscience, Hoboken, N.J, 2004.

Tables

Table 1: properties of water and Isane employed in the emulsification experiments

Product \ property	**density (ρ, kg/m^3)**	**viscosity (μ, Pa.s)**	**surface tension (N/m)**
water	997.8	0.001	0.0383
Isane	762	0.0012192	

Table 2: Averaged turbulent dissipation rates $\bar{\varepsilon}$ (m^2/s^3) according to correlation (eq. 26) and by CFD simulations (water-isane,).

Method \ stirring rate	**$\bar{\varepsilon}$ at 600 rpm**	**$\bar{\varepsilon}$ at 700 rpm**	**$\bar{\varepsilon}$ at 800 rpm**
Averaged $\bar{\varepsilon}$ (using Eq. 26)	0.63	1.01	1.47
CFD (using water as continuous phase)	0.64	1.01	1.50
CFD (using Isane as continuous phase)	0.61	0.99	1.49

(4.3) Table 3: Reynolds numbers for Isane continuous-phase experiments (first row) and water continuous-phase experiments (second row) at different rotational speeds of the impeller.

Phase \ Reynolds number	**600 rpm**	**700 rpm**	**800 rpm**
Isane	22500	26500	30000
Water	36000	42000	48000

Table 4: Volume-averaged turbulent dissipation rates $\bar{\varepsilon}$ (m^2/s^3) in the recirculation zone, in the impeller zone and in the total volume for water-phase CFD simulations.

Stirring rate \ zone	**$\bar{\varepsilon}$ in the impeller zone**	**$\bar{\varepsilon}$ in the recirculation zone**	**$\bar{\varepsilon}$ in the reactor**
600 rpm	2.17	0.51	0.64
700 rpm	3.37	0.83	1.01
800 rpm	5.19	1.21	1.51

Table 5: Identified parameters for the Coulaloglou and Tavlarides kernel employing the pdf of ε or assuming a uniform value.

	Breakup		**Coalescence**	
	C_1	**C_2**	**C_3**	**C_4**
pdf of ε	1.20×10^{-3}	7.11×10^{-1}	1.95×10^{-2}	2.05×10^{14}
uniform ε	7.84×10^{-2}	3.06×10^{-1}	3.75×10^{-4}	8.23×10^{18}

Figures

Fig. 6: Example of image treated through the SOPAT software. The half bottom image represents the photographed droplets. The half upper, the detected ones, enlightened by green circles.

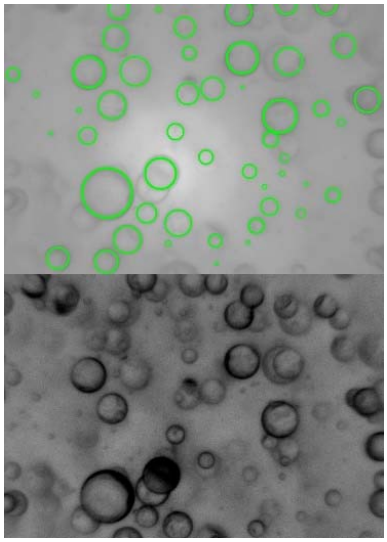

(2.2) Fig. 7: Probability density functions, f(ε) for water (left) and Isane (right) at different impeller rotational speeds (600-700-800rpm).

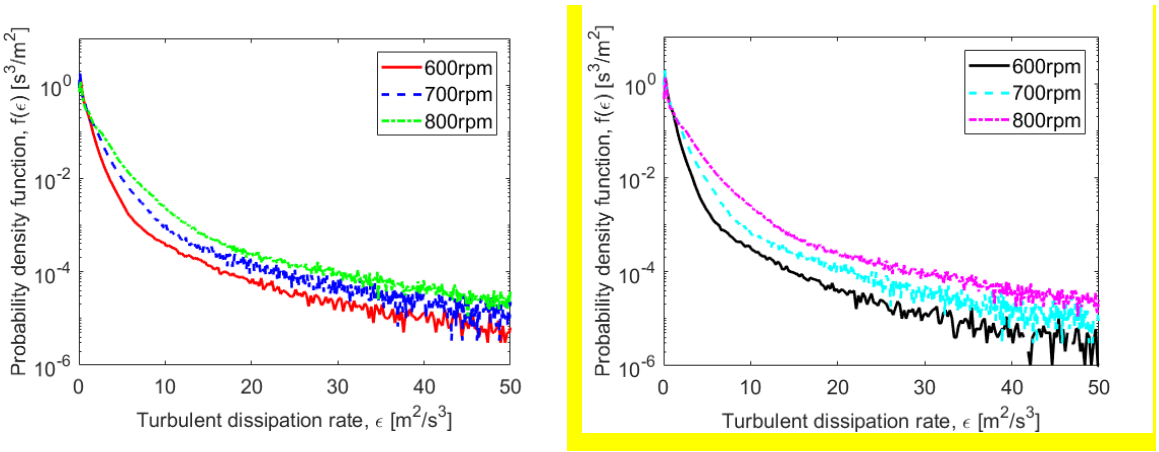

(2.3) Fig. 3: Comparison of the probability density functions for Isane and water at 600rpm (top-left), 700rpm (top-right), 800rpm (bottom).

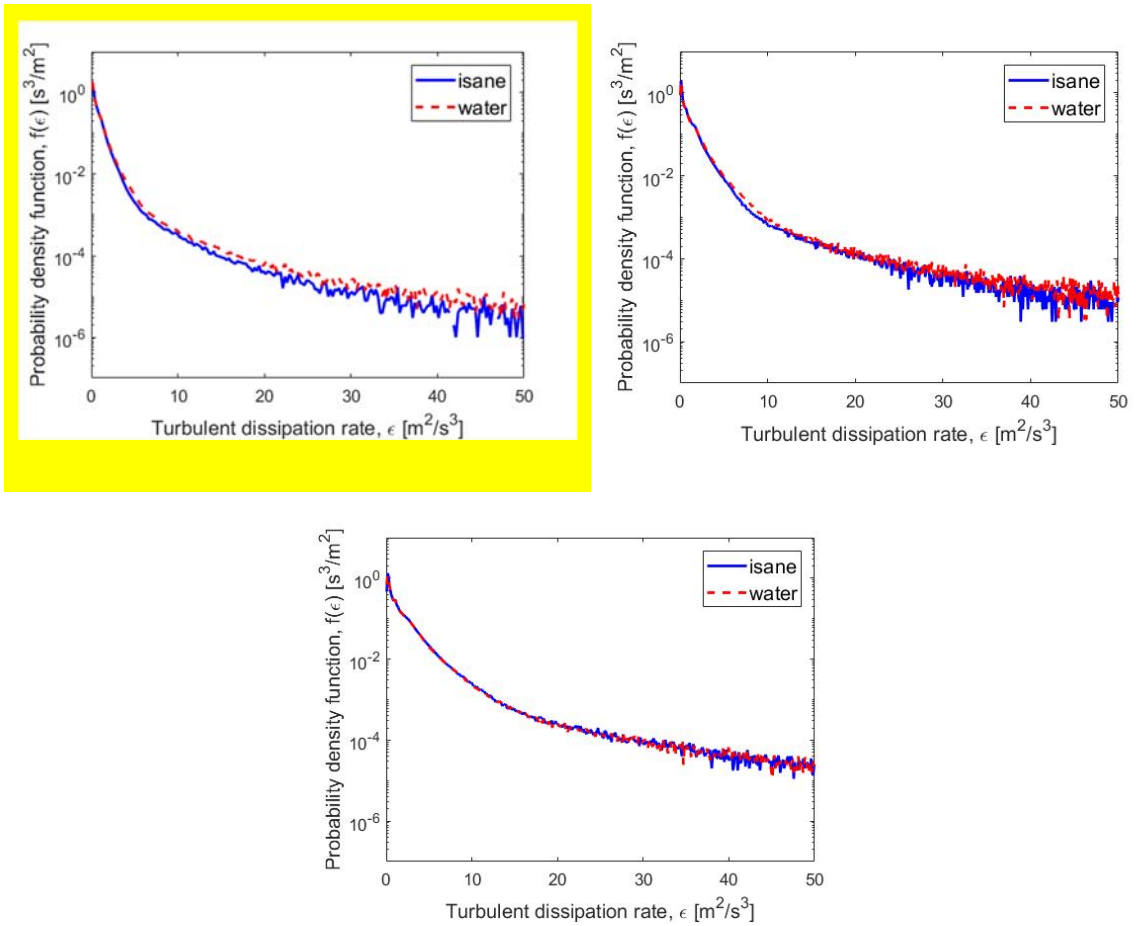

Fig. 4: Space distributions of the turbulent dissipation rate, ε (m^2/s^3), at 600 rpm (left), 700rpm (center), 800 rpm (right) according to water-phase CFD simulation.

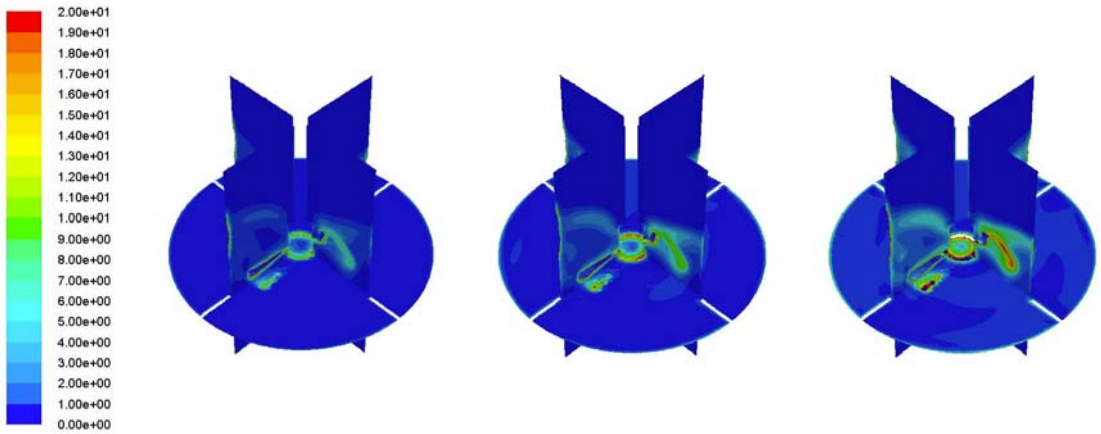

Fig. 8: Time evolution of the droplet Sauter mean diameters for oil-in-water experiments at 1% (left) and 2% (right) volume fraction of Isane hold-up and 600rpm, 700rpm and 800rpm.

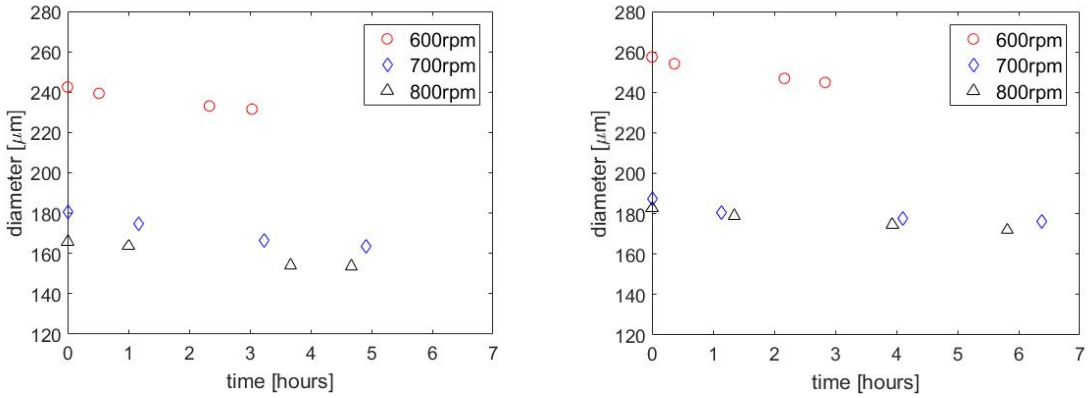

Fig. 9: Time evolutions of the droplet Sauter mean diameters for the water-in-oil experiments at 1 % volume fraction of water hold-up and 600rpm, 700rpm and 800rpm.

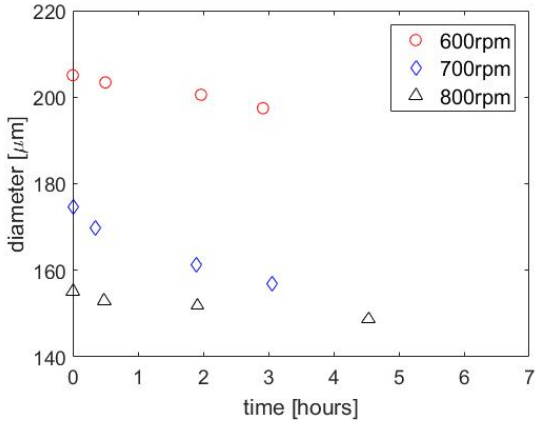

Fig. 10: Time evolutions of droplet Sauter mean diameters for oil-in-water (empty) and water-in-oil (plain) experiments at 1% disperse phase hold-up and at 600rpm (red) 700rpm (blue) and 800rpm (black) rotational speeds

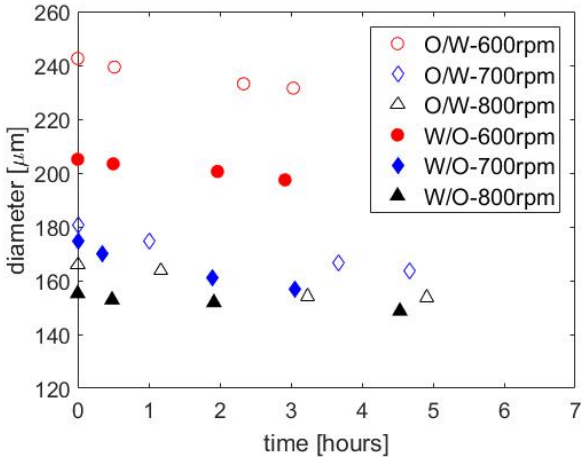

Fig. 11: Parameters identification on oil in water experiments at 1% (circles) and 2% (rhombus) of Isane hold-up employing the pdf (blue) or assuming a uniform value (black) of ε.

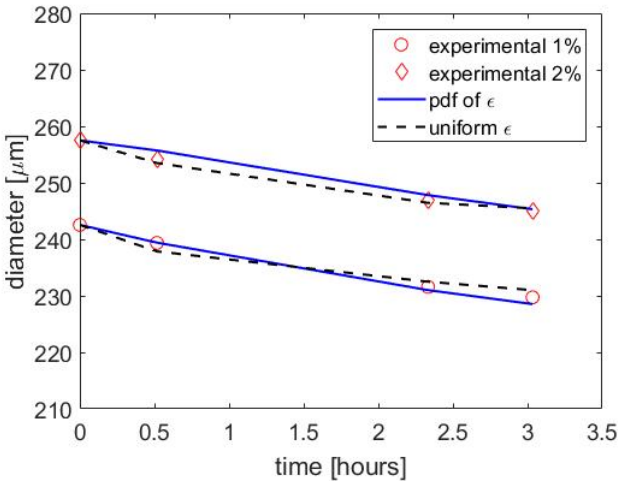

Fig. 12: Parameters testing on oil-in-water experiments at 1-2 % of Isane hold-ups employing the pdf or assuming a uniform value of ε.

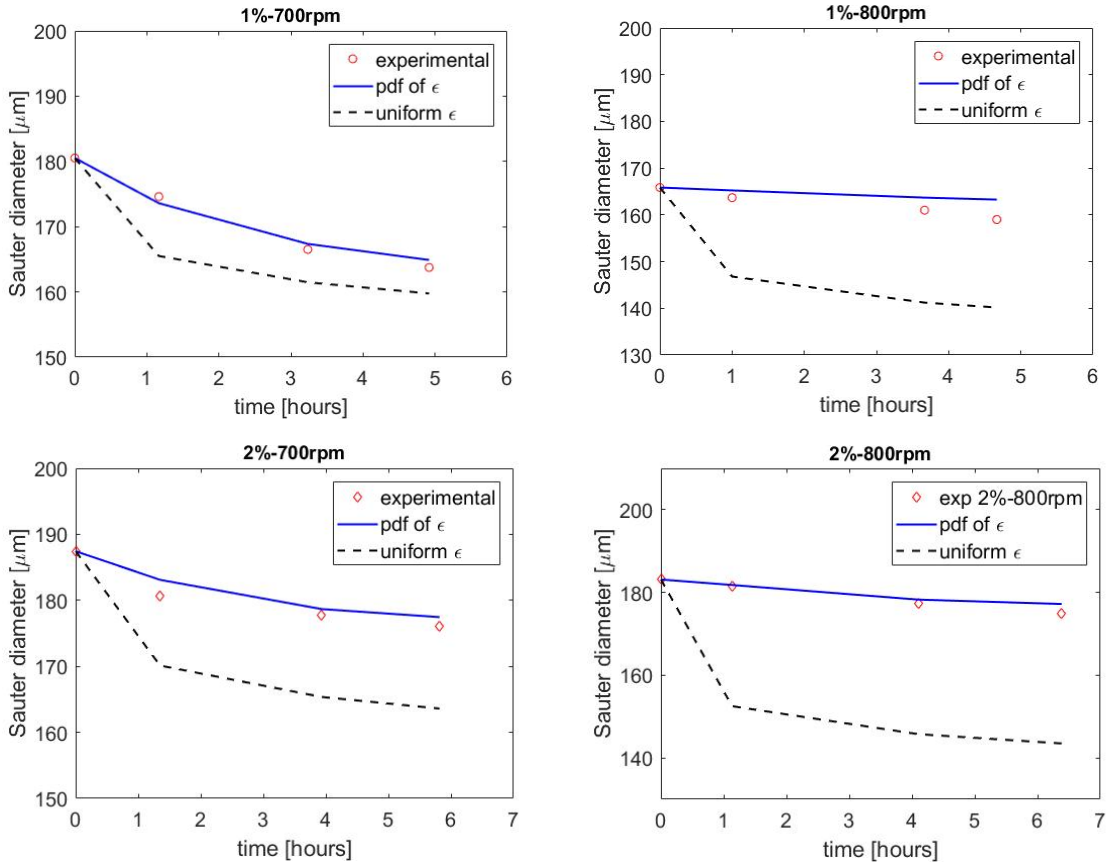

Fig. 13: Parameters testing on oil-in-water experiments at 1% volume fraction of water hold-up employing the pdf or assuming a uniform value of ε.